Chinese Journal of Aeronautics, (2019), 32(11): 2443–2454

Chinese Society of Aeronautics and Astronautics
& Beihang University

Chinese Journal of Aeronautics

cja@buaa.edu.cn
www.sciencedirect.com

Investigations of tip-jet and exhaust jet development in a ducted fan

Lei LI *, **Guoping HUANG**, **Jie CHEN**

College of Energy and Power Engineering, Nanjing University of Aeronautics & Astronautics, Nanjing 210016, China

Received 19 September 2018; revised 13 November 2018; accepted 20 November 2018
Available online 31 May 2019

KEYWORDS

Blade circulation;
Blade solidity;
Exhaust jet;
Fans;
Tip-jet

Abstract The major aim of this work is to investigate the tip-jet and exhaust jet development in a ducted fan as well as the impact on the fan's performance. The flow field of the ducted fans under the solidity varied from 0.2 to 0.7 are simulated by using the shear-stress transport k-ω turbulence model with a refined high-quality structured grid. The exhaust jet trajectory, expanding range and the flow intersection of the jet and mainstream in the blade passage are analyzed. As the results suggest, the flow direction of the exhaust jet is deflected by the downwash and Coanda effect. The major decay region of the exhaust jet can extend at least 2 times the blade chord downstream from the blade trailing edge. The blade circulation is impacted by the tip-jet rather than the exhaust jet from the upstream when the blade tip pitch angle is 8°, and the fan solidity is less than 0.7. The blade tip thrust is reduced by the interruption from the exhaust jet when the blade tip pitch angle is 2°, and the fan solidity is larger than 0.3.

© 2019 Chinese Society of Aeronautics and Astronautics. Production and hosting by Elsevier Ltd. This is an open access article under the CC BY-NC-ND license (http://creativecommons.org/licenses/by-nc-nd/4.0/).

1. Introduction

Tip-jet rotor, driven by the reaction torque produced by the jet ejected out of the nozzle at the blade tip, serves as a potential propulsion unit in the vertical take-off vehicles. Friedrich von Doblhoff[1] is considered the first engineer to realize the potential significance of the tip-jet and tried to invent a novel type of air vehicle. He designed the first prototype of the tip-jet aircraft WNF-342 and made its maiden flight in the 1940s. This type of rotor was advantaged in the simple structure and light gross weight since the pneumatic reaction-drive rotor did not need the anti-torque and reduction gearbox systems. To study and examine the ability of the tip-jet driven rotors, a large number of explorations were made during 1950s. In the early research, the engine was mounted at the blade tip to produce the jet, probably resulting in a serious structural problem and loud noise. Then, bleeding the energetic air from a gas generator to the blade tip brought the research to the next level. A successful aircraft built to validate this technology was the XV-9A, a type of combination aircraft with the fixed wing and rotors. Besides, given that the magnitude of the weight growth is incredible with the increase of the aircraft's volume, some researchers sought to employ the tip-jet rotor in the heavy transport aircraft field. For instance, the Fairey Rotodyne tip-jet aircraft flown in 1957 was designed as a commercial plane with the capacity of forty passengers. However,

* Corresponding author.
E-mail address: michaelleili@hotmail.com (L. LI).

Peer review under responsibility of Editorial Committee of CJA.

Production and hosting by Elsevier

https://doi.org/10.1016/j.cja.2019.04.026
1000-9361 © 2019 Chinese Society of Aeronautics and Astronautics. Production and hosting by Elsevier Ltd.
This is an open access article under the CC BY-NC-ND license (http://creativecommons.org/licenses/by-nc-nd/4.0/).

the study of tip-jet rotor was gradually slowed down since its application was limited by the noise and high fuel consumption levels at the time and the control problem of the rigid rotor. Until the research into the VTOL (Vertical Take-Off and Landing) aircraft[2,3] rose in 1990s, a new approach was developed by integrating the tip-jet with other technologies. For instance, the Boeing X-50A flown in 2003 was a Canard rotor wing concept aircraft. It had a tip-jet rotor to lift and the exhaust nozzles working during the vertical take-off and landing period and high speed cruising, respectively.[4,5]

To re-estimate the utility of the tip-jet in helicopters, Phillips[6] consulted the improved technology of the modern gas generator. As he suggested, during the hover time of a tip-jet helicopter had the larger overall efficiency than the shaft drive when the gross weight was over 36400 pounds. This was benefited from the cold cycle technology that could reduce the speed of the exhaust jet. Schwartz et al.[7] tried to design a new aircraft using the tip-jet rotor to take off. Following this concept, the power resource of the bleeding air originated from a turbofan. They also investigated[8] the aerodynamic characteristic of a tip-jet rotor with circulation control. As the result suggested, the system efficiency was impacted by the nozzle region at the blade tip. Under some specific conditions, jets ejected out of the wing's trailing region could introduce energy to the shed vortex and make it diminish rapidly.[9] Elmahmodi et al.[10] performed a test of the tip-jet from a rocket motor. A high payload for flight of this tip-jet rotor was shown. The acoustic analysis of the tip-jet rotor was conducted by Brentner et al.[11] in 2014. As the result suggested, the variation of the nozzle outlet area was susceptive to the tip-jet noise. The recently research has suggested the ducted fan or fan-in-wing device was effective in the VTOL aircrafts. The flow control technology could help to improve the aerodynamic performance of the aircrafts.[12–14] Our previous work[15] studied the basic aerodynamic behavior of a ducted fan with tip-jet. Based on the idea of combining the pneumatic drive and flow control simultaneously, the previous results suggest that placing the nozzle at the suction surface of the blade could improve the blade circulation using the exhaust jet. This flow impact was similar to the circulation control used broadly in the fixed wing aircraft.[16] However, the fan profile studied in our previous work was based on an untwisted NACA0012 airfoil[17] with two blades. This might not be representative since typical ducted fan blades have high twist and solidity to create high disk loadings.[18] Accordingly, whether the exhaust jet could create a strong disturbance and turbulent flow inside the blade passage of a high solidity fan and then result in a poor overall performance was of great significance to evaluate the utilization of the tip-jet into a ducted fan. To clearly illustrate the mechanism of the impact of the exhaust jet, a detailed study of the exhaust jet development, flow structures and aerodynamic performance has been conducted and presented systematically in this paper. Section 2 introduces the concept of the ducted fan with tip-jet system, followed by the detailed descriptions of the configuration of the ducted fan with tip-jet. Section 3 then presents computational method. The section of results and discussions presents the exhaust jet expanding region and the flow features. The comparison of the aerodynamic performances (thrust coefficient, power coefficient and fan's figure of merit is to be analyzed. Finally, the essential findings are summarized, and some conclusions are drawn in Section 5.

2. Description of ducted fan with tip-jet

The conceptual diagram of the ducted fan with tip-jet is given in Fig. 1. It serves as a highly effective propulsion unit to turn the thrust direction of the core engine and meanwhile augment it. The low weight cost and complexity of this fan can support an aircraft to vertical take-off with an acceptable fuel consumption.

The configuration of the open fan in this paper is referenced from a test model investigated at the U.S. Naval surface warfare center, Carderock division.[19,20] This open fan was tested as an isolated fan and in a fan-in-wing system to improve the understanding of the fluid dynamic interactions between a fan and wing. This research was under the interest in the vertical takeoff and landing. Since the experiment data covers a wide range of rotational frequencies and pitch angles, it can serve as an open fan model in this paper. The diagram of the open fan is given in Fig. 2. This fan is composed of six distributed, rectangular and symmetric NACA0012 rigid blades. The blades have a total twist angle of negative 12° from the hub to the tip, a flat tip surface as well as a round trailing edge. The blade in the wind-tunnel test model is attached to the blade spindle, allowing the change of the blade pitch angle. Also, it is bolted to the fan hub. To simplify the computational model, a cylinder with a diameter of 5.5 in (1 in = 2.54 cm) is designed to replace the real hub system. The detailed parameter information of the fan is listed in Table 1. To explore the impact of the fan solidity, in accordance with the same blade model, the blade number is increased from 6 to 12, 16, 18 and 20. Correspondingly the fan solidity (σ) is increased from 0.218 to 0.437, 0.580, 0.655 and 0.728, respectively. The image of the fans with various solidities is shown in Fig. 3. The numerical computation for the fans in hover are performed at two different rotational frequencies (ω_r = 3700,6300 r/min) and two different pitch angles (θ = 2°, 8°). The ambient temperature (T_∞) and pressure (p_∞) are 288.15 K and 101300 Pa, respectively. The detailed operating and reference conditions for the numerical experiment are listed in Table 2, where v_{tip} is the blade tip speed.

As this paper is focused on the flow interaction inside the fan, a geometrically regular duct is designed for the ducted fan system. Section profile of the duct lip is designed to has a semicircular curve and the tip clearance is 3 mm. A nozzle and an internal pipe are mounted inside the blade for simulating the bleeding process like the real situation. The inlet of the internal pipe is placed at the blade root. From the inlet of the

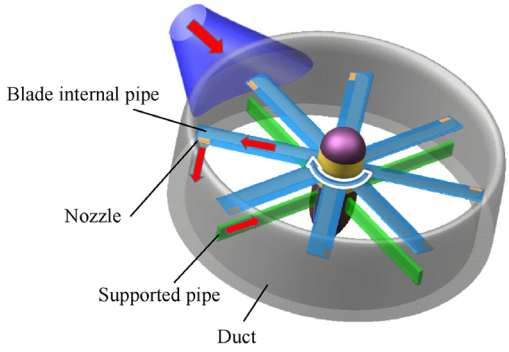

Fig. 1 Ducted fan with tip-jet configuration.

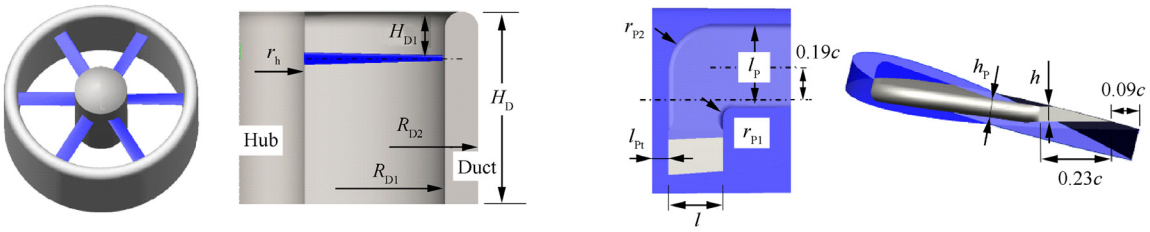

(a) Duct (b) Internal pipe

Fig. 2 Computational model.

Table 1 Geometric information about ducted fan with tip-jet configuration.

Parameter	Symbol	Value
Blade radius	R_1 (mm)	301.625
Blade chord	c (mm)	50.8
Hub radius	r_h (mm)	96.8
Duct height	H_D (mm)	285
Duct inlet height	H_{D1} (mm)	70
Duct inner radius	R_{D1} (mm)	305
Duct external radius	R_{D2} (mm)	355
Pipe width	l_P (mm)	22.8
Pipe height	h_P (mm)	3.16
Pipe inner corner	r_{P1} (°)	2.88
Pipe external corner	r_{P2} (°)	12.8
Nozzle outlet length	l (mm)	15
Nozzle tip distance	l_{Pt} (mm)	4.5
Nozzle height	h (mm)	2.5

internal pipe, a constant section, a turning, a contraction and a rectifying section are to connect to the nozzle in sequence. The function of the rectifying section is to lead the jet flow horizontally (parallel to the rotational plane) to the nozzle outlet. The nozzle could be called conformal nozzle with no variation on the blade profile when its outlet is closed. Furthermore, the nozzle is opened at the suction surface of the blade and near the blade trailing. The detailed parameter information of the duct and internal pipe are listed in Table 1.

3. Numerical method and validation

The software ANSYS CFX based on the finite volume method to solve the Navier-Stokes equations is applied in this paper. The steady simulation is used for obtaining the fan's characteristic and the basic flow field in this paper. As the shear stress and compressibility of fluid could be significant at the interaction region, the turbulence model of Shear-Stress Transport (SST) k-ω[21–23] is performed in this paper. During all computations, the high resolution is selected for the advection scheme and numerics option items.

3.1. Numerical setup

The structured hexahedrons grid is built for computational models. The final grid number magnitude of the cases with 6 blades have 6.9 million cells. The section of internal pipe is meshed with O-grid. Besides, the O-grid is applied in the tip region for acquiring a high grid quality. The pipe domain and blade domain are connected by an interface. The display of the grid image of the computational domains is shown in Fig. 4.

The pressure and temperature boundary conditions are applied in the far-field inlet and outlet. The edge of the far-field is ten times the rotor radius from each direction. The atmosphere pressure and temperature far from the rotor are 101300 Pa and 288.15 K, respectively. All the wall's boundary

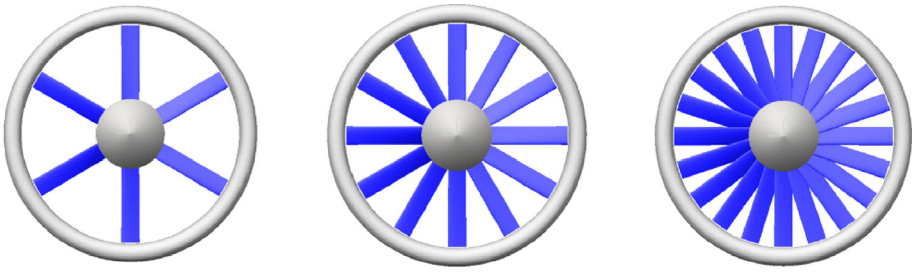

σ=0.218 σ=0.580 σ=0.728

Fig. 3 Fans with different solidities.

Table 2 Operating and reference conditions.

ω_r (r/min)	v_{tip} (m/s)	Fan solidity	Blade number	p_∞ (Pa)	T_∞ (K)	θ(°)
3700	117	0.218, 0.437, 0.582, 0.655, 0.728	6, 12, 16, 18, 20	101300	288.15	2, 8
6300	199	0.218, 0.437, 0.582, 0.655, 0.728	6, 12, 16, 18, 20	101300	288.15	2, 8

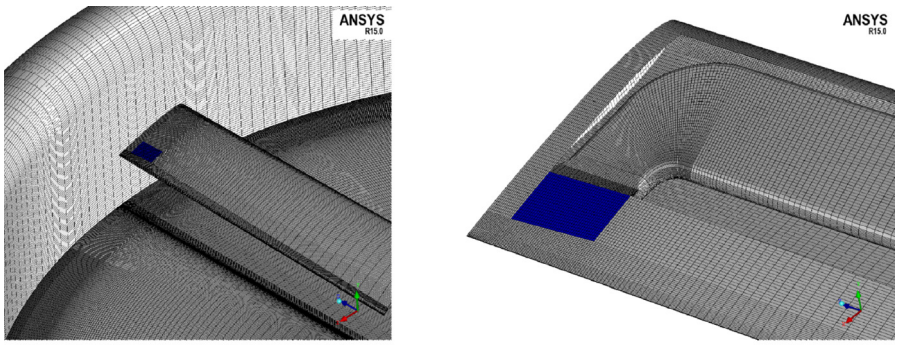

(a) Around duct and blade (b) Around internal pipe

Fig. 4 Structured grid.

conditions are no slip wall and adiabatic. Periodic surface is selected to save the computational cost for a single blade passage. To reduce the number of the boundary variable, the bleeding air with 400 K total temperature is applied for all the cases. Only the total pressure of the bleeding air is changed in various cases. Within a steady simulation, the frozen-rotor interface is selected between the rotational and stationary domains, and the multiple frames of reference method is adopted. The residual targets are set to less than 1×10^{-4} (continuity, heat transfer, momentum, turbulence quantities and a monitor variable). For the cases of the ducted fan without tip-jet, the convergence of the solution is achieved after 1500 iterations and the monitor value of the mass flow rate is stable. However, an available case of the ducted fan with tip-jet is the balance of the blade's torque to the jet's torque. Thus, the solution convergence of these cases is achieved when the difference is close to 0 between the blade's torque to the jet's torque.

3.2. Grid-resolution study

The grid size plays an important role in the accuracy of the CFD results. A grid independence study is normally necessary before large amounts of simulations for checking the validation and optimizing computational cost. Three different types of meshes for the open fan are employed: a coarse grid of 3.7×10^6 nodes, a medium grid of 6.9×10^6 nodes and a fine grid of 13.8×10^6 nodes. Relevant dimensions and spacing of the grids are listed in the Table 3. The grid refinement is performed in the blade's streamwise direction, especially on its rear part to increase the mesh density in the region of the jet mixing with the mainstream. Subsequently, the refinement is made in the blade's spanwise direction and the points wrapping around the blade. The grid refinement has a slight influence on the overall aerodynamic coefficient. The relative difference between the fine and medium grids is nearly 1% for the thrust and power coefficient, as listed in Table 3. The coarse grid predicts a satisfactory result of the aerodynamic coefficient. However, the medium grid provides an improved resolution of the flow visualization pictures with a small computation time increment. Accordingly, the medium grid size is applied for the configurations with 6 blades. The y^+ on the blade surface is created to be near 1. On the wall of the duct, the y^+ is less than 5. As a single blade passage is built for a periodic calculation, the normal and circumferential layers are decreased proportionally to the increased blade number of other cases. Yet the warp around points, spanwise layers and spacing are the same as the medium grid type.

Table 3 Details of grid employed for open fan.

Parameter	Value		
	Coarse grid	Medium grid	Fine grid
Warp around points	86	106	136
Spanwise layers	120	150	180
Normal layers	80	110	140
Circumferential layers	130	160	200
Spacing on the blade surface/c (10^{-4})	1.3	1.0	0.8
Total number of nodes (10^6)	3.7	6.9	13.8
Thrust coefficient	0.03454	0.03421	0.03401
Power coefficient	0.00932	0.00927	0.00924

3.3. Numerical validation

The aerodynamic performance of the open fan using the numerical experiment method is validated by comparing it with the experimental data obtained by Bi et al.[20] with work presented at the AHS 71st annual forum. The experimental data was yielded for a wide flow range of the rotational frequencies, solidities and pitch angles and gathered in a subsonic wind tunnel. The fan was operated in hover condition and the test section static pressure was one atmosphere. The numerical computation result of the open fan operating at 3700 r/min with the pitch angle ranged from 7° to 46° is selected for comparison with the experimental data. The comparison of the blade thrust coefficient (C_T) versus power loading coefficient (C_Q) between the numerical computation and experimental results is shown in Fig. 5. As suggested from Fig. 5, the C_T/σ rises quickly with the increase of the C_Q/σ from 0 to 0.06 and then declines slowly to the stall margin. Due to the difference between the wind tunnel and free air in the simulation and the difference of the simplified hub and blade in details, the trend of the predicted C_T/σ is a little higher than that of the test data. The maximum discrepancy between the CFD and test results is less than 5%, suggesting an acceptable accuracy for further discussion.

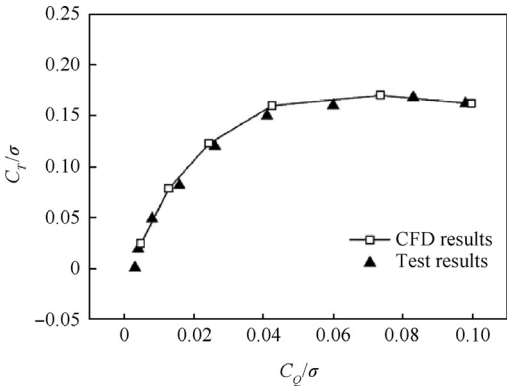

Fig. 5 Comparison of aerodynamic coefficient of open fan between test and CFD results.

4. Results and discussion

The investigation of the ducted fan with tip-jet as well as a series of fan solidities operating under two rotational frequencies in hover is performed using the numerical experiment. A comparable case without the tip jet (reference case) is performed under the same conditions as the tip-jet case for comparison to better understand the aerodynamic interaction between the jet and mainstream.

4.1. Development of exhaust jet

The computational cases of the ducted fan with 6 blades are selected to present the exhaust jet development. To get a first impression of the exhaust jet at the blade downstream region, the Mach number (*Ma*) contour of a fan with a blade tip pitch angle of 2° is shown in Fig. 6(a). The plane "A" in Fig. 6(a) has the same pitch angle as the blade tip and cut through the half part of nozzle. Fig. 6(a) shows that, the highest speed path of the exhaust jet is close to the nozzle edge in blade tip direction due to a relatively high local pressure difference and the centrifugal force. Besides, this highest speed path is shifted by the tip and shed vortices. Obviously, the exhaust jet is non-uniform in space and intersected with the unsteady turbulences in the blade passage. Nevertheless, the exhaust jet can maintain a major flow region which can reflect the jet evolution and trajectory. To obtain a qualitative understanding of the impact of the exhaust jet and to obtain the magnitude of such impact on the fan's overall performance, the steady solution could be sufficient.

As shown in Fig. 6(a), a central path of the exhaust jet can be drawn by following the maximum speed of the exhaust jet on the plane A. Subsequently, the approximate radius of this path can be identified (r is the radius and R is the blade radius). To investigate the farthest expanding edge of the exhaust jet, the speed parameter at a cylinder surface with the same radius of the central path is extracted to show the speed development of the exhaust jet. The definition of the relevant direction parameters is given in Fig. 6(b). The y-axis and circumferential line are vertical and parallel to the rotational plane, respectively.

The flow behavior at several downstream locations on the cylinder surface is shown in Fig. 7. Where v and v_r denote the velocity from the tip-jet and reference cases, respectively; d_y is the axial distance from the blade trailing edge and d_{cir} is the circumferential distance from the blade trailing edge. Fig. 7 also suggests that the maximum velocity ratio between

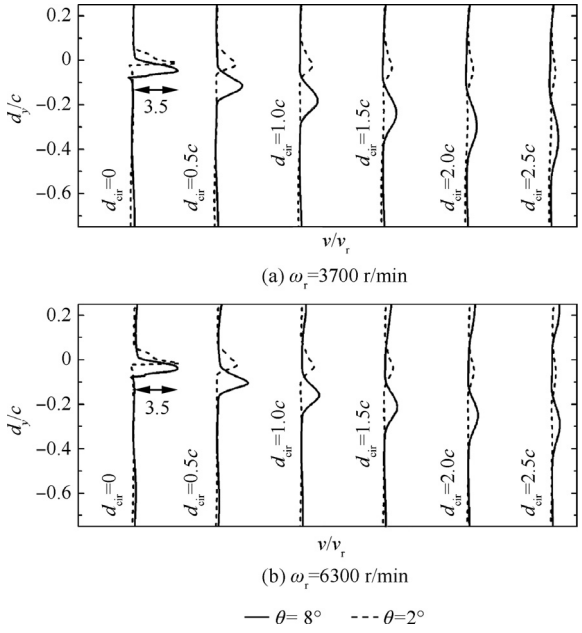

Fig. 7 Exhaust jet development.

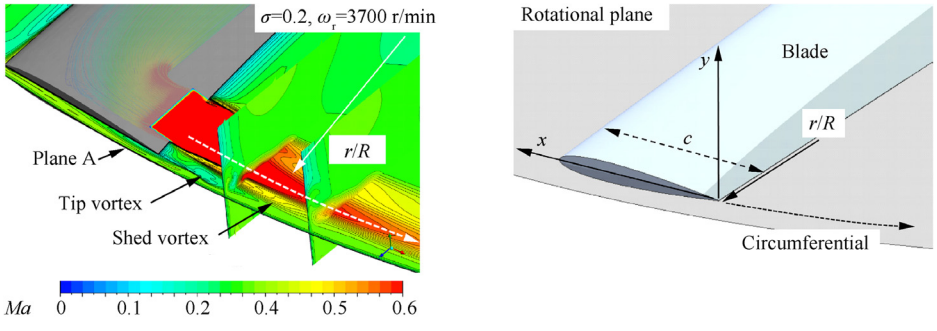

(a) Mach number distribution (b) Direction parameters definition

Fig. 6 Flow field visualization of fan with tip-jet.

the tip-jet to the reference case is nearly 3.5 just behind the blade trailing edge. The peak value position of the velocity ratio moves down gradually since the distance from the blade trailing edge increases in the downstream direction. It is suggested that the exhaust jet turns the flow direction after being ejected out of the nozzle. Such deflected angle is nearly 2° smaller than the local pitch angle. This deflection is formed by the Coanda effect and downwash. More discussion concerned with this flow phenomenon is to be presented in the following section.

The dimensionless decay curve of the exhaust jet central trajectory is plotted in Fig. 8(a). The central trajectory of the exhaust jet is defined as the trajectory of the maximum speed of the exhaust jet. Where d is the space distance from the blade trailing edge, d_{jy} is the normal distance from the central trajectory of the exhaust jet. Though the pitch angle and rotational frequency are different, the similar decay trend is found in Fig. 8(a). The exhaust jet region could fall into a major decay region and an inertial decay region. The major decay region can extend 2 times the blade chord downstream of the blade in which the decline of the jet velocity is quick. On the other hand, the jet velocity has a slow decline, and the velocity ratio is lower than 1.5 in the inertial decay region after the major decay region. It is speculated that the margin of the exhaust jet influence region could reach a distance of 3.5 times the blade chord in the downstream direction. The spreading width of the exhaust jet along the central trajectory is shown in Fig. 8 (b). The expanding of the jet along the central trajectory is not completely symmetric for the pressure difference on the two sides of the rotational plane. When the d/c is 2.0, the margin of the jet decay in width is nearly $0.1c$. When the d/c is larger than 2.0, the velocity ratio is smaller than 1.5.

Based on the analysis of the development law of the exhaust jet, the influence region of the exhaust jet in a higher solidity fan could be generally predicted. As shown in Fig. 9, the fan solidity and blade tip pitch angle are assumed to be 0.7 and 8°, respectively. Where z is the blade number, LE is the blade leading edge and TE is the blade trailing edge. The exhaust jet trajectory and its expanding area could be predicted by consulting the data from Figs. 7 and 8. The gray area in Fig. 9 is a velocity profile in which the velocity ratio between the tip-jet and without tip-jet cases exceeds 1.5. As the jet flow has a deflection angle towards the fan outlet, the exhaust jet could pass under the blade in the downstream direction, as shown in Fig. 9. Accordingly, the impact of the exhaust jet on the downstream blade could be marginal if the fan solidity is smaller than 0.7 and the tip pitch angle is 8°. To verify this prediction, the following section will show the detailed flow field and reveal the quantitative impact of the exhaust jet on the blade circulation.

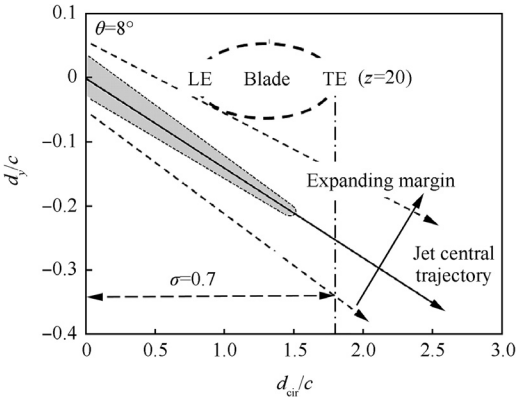

Fig. 9 Estimation of exhaust jet development.

4.2. Impact of tip-jet and exhaust jet

(1) Blade tip pitch angle: $\theta = 2°$

In this section, the mechanism of the impact of the tip-jet and exhaust jet on the fan's aerodynamic behavior is to be presented. Fig. 10 displays the Mach number contour on a cylindrical surface passing the center of the nozzle in the spanwise direction. It is noteworthy that the flow below the pressure surface of the blade is accelerated by the exhaust jet under 20 blades, corresponding to $\sigma = 0.7$. This impact results in a reduction of the pressure below the blade pressure surface. To reveal the impacted area on the blade, the pressure coefficient (C_p) distribution on the blade surface is displayed in Fig. 11, where SS and PS represent the suction surface and pressure surface of the blade, respectively. Besides, Ref. represents the reference blade/fan.

Fig. 11 suggests that the low pressure area on the suction surface of the blade with tip-jet is larger than that of the reference blade in both 6 and 20 blades cases. The pressure on the pressure surface near the leading edge of the blade with tip-jet

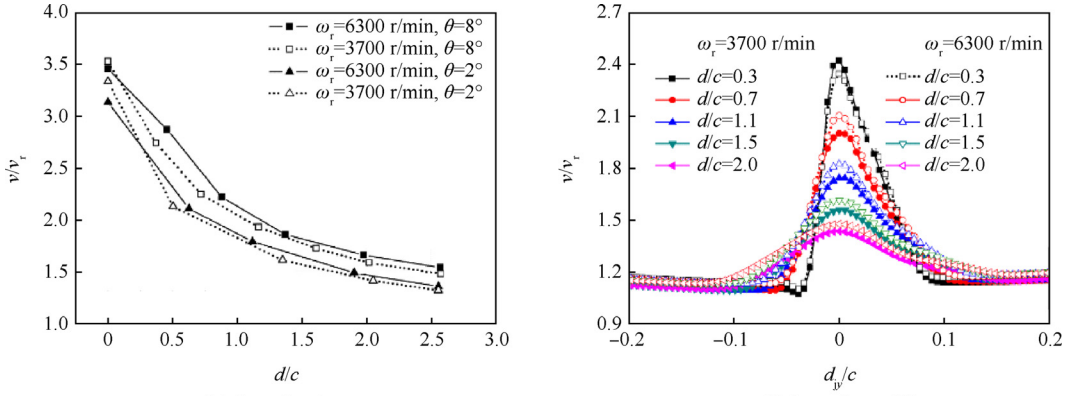

(a) Central trajectory (b) Spreading width

Fig. 8 Dimensionless decay of exhaust jet velocity.

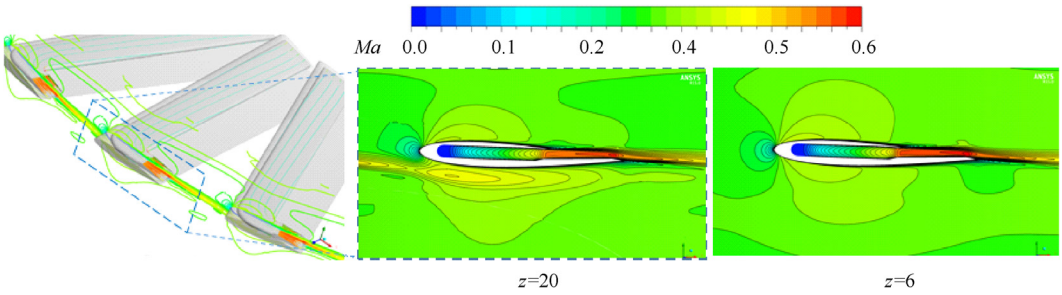

Fig. 10 Mach number contour around blade ($\theta = 2°$, ω_r = 3700 r/min).

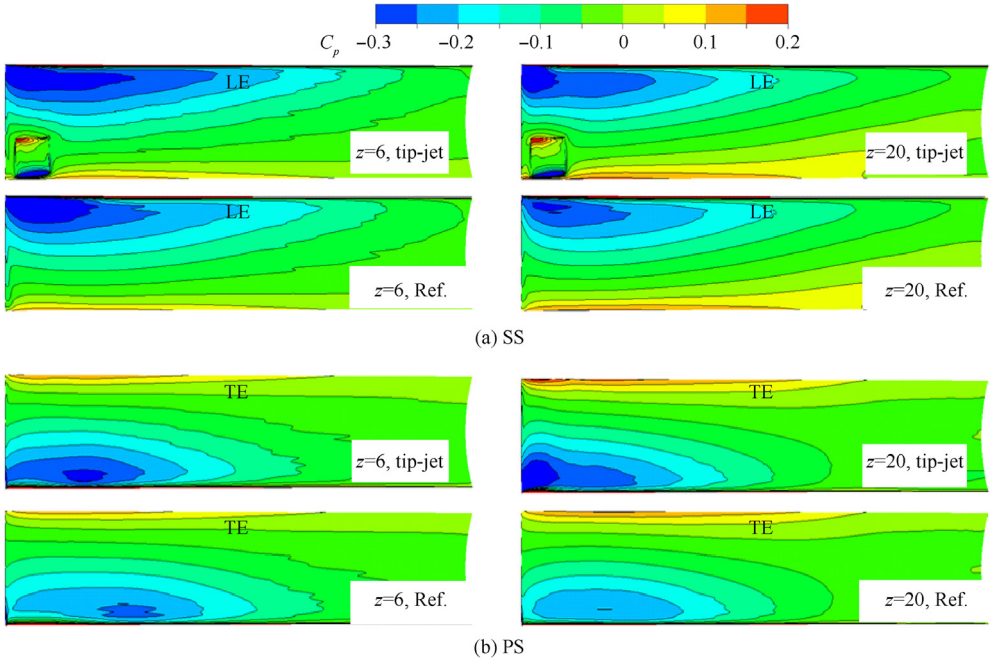

Fig. 11 Pressure distribution on blade surface ($\theta = 2°$).

is lower than that on the reference blade in both 6 and 20 blades cases. The exhaust jet is shown to entrain the flow in the upstream direction at a certain span region from the blade tip. The speed of the mainstream at the blade front part is accelerated to obtain the energy from the exhaust jet. Obviously, the lowest pressure area on the pressure surface of the blade with tip-jet moves to the tip direction under 20 blades. As mentioned above, the central trajectory of the exhaust jet is close to the blade tip and has a reflection angle to the down side of the blade. The pressure in the wake region of the jet exhaust is relatively lower. Thus, the lowest pressure area on the pressure surface of the blade in the downstream direction is affected more as a closer distance between the blades.

To reveal the lift distribution on the blade sections, the mean pressure coefficient at the different spanwise sections of the blade is shown in Fig. 12. Lines with solid and hollow symbols represent the mean pressure coefficient at the blade pressure and suction surfaces, respectively. $r^* = (r - r_h)/(R - r_h)$ is the spanwise ratio. When the blade number is 20, the major difference of the pressure distribution on the blade between the tip-jet and reference cases take up 25% spanwise range from the blade tip. Pressure on the suction and pressure surfaces of the tip-jet blade at this region are both lower than those of the reference case for the entrainment impact. Obviously, a relatively low pressure area occurs on the suction surface of the blade within the nozzle spanwise region for the nozzle on the suction surface of the blade. However, this lowest pressure area on the suction surface of the blade is not further extended in the hub direction. Hence, the pressure difference is reduced between the suction and pressure surfaces of the blade in 0.82–0.87 spanwise region, and the flow below the pressure surfaces is also accelerated.

Under 6 blades, the pressure distribution on the blade between the tip-jet and reference cases is different in the whole blade spanwise region. The pressure on the suction surface is lower than that of the reference case for a wide blade spanwise region. The pressure on the pressure surface of the blade with tip-jet is higher than that of the reference case in 0.3–0.75 spanwise region, indicating that the lift of the blade with tip-jet is enlarged in this region. The jet is shown to entrain the flow at a large spanwise region of the blade when the pitch angle and fan solidity are both small. It could be due to the control of the blades to the mainstream in the blade passage is weak at a lower fan solidity. Then, the impact of the exhaust jet to the

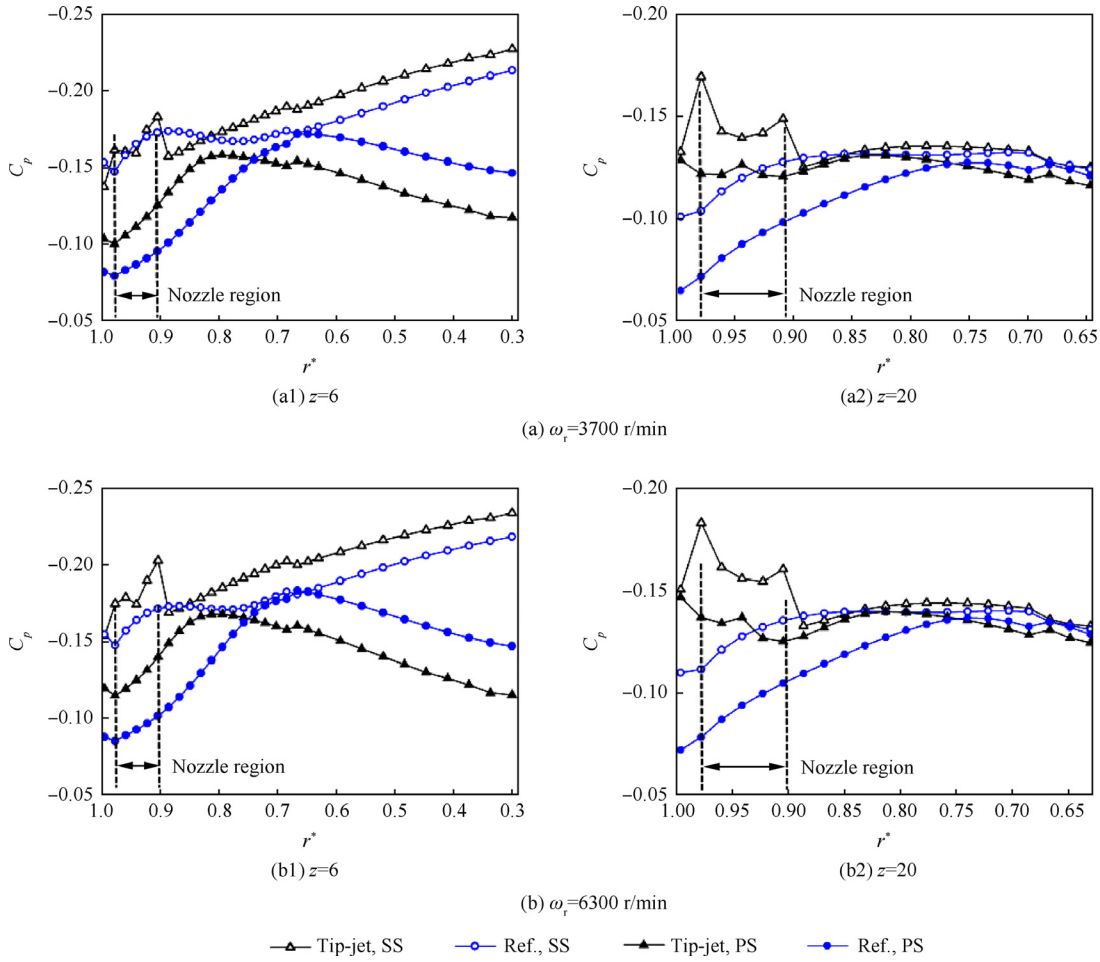

Fig. 12 Pressure distribution at blade spanwise direction ($\theta = 2°$).

mainstream is more obvious in a large blade spanwise region. The character of the pressure distribution in these cases changes slightly at ω_r = 6300 r/min.

Three different blade spanwise sections, i.e., near the tip (r^* = 0.99), at the nozzle center (r^* = 0.94) and at the position of r^* = 0.85, are selected to present a detailed information of the pressure distribution around the blade, as shown in Fig. 13. A high pressure region is found occurring at the upstream of the nozzle and on the suction surface of the blade, in which the flow is blocked by the flow intersection between the exhaust jet and mainstream. Since the exhaust jet crashes into the mainstream pushing down from the blade upstream direction. Another critical feature happens at the nozzle downstream and on the suction surface of the blade, in which the pressure is dropped due to the Coanda effect. Due to the balance between the centrifugal force and pressure difference on the fluid, the exhaust jet is attached to the curved surface. This pressure reduction area contributes to the rise of the blade local lift.

In brief, the lift of the blade with tip-jet can be augmented in a wide blade spanwise range since the exhaust jet entrains the mainstream above the suction surface of the blade in a large spanwise region when the fan solidity and local pitch angle are both low. While the distance between the blades reduces with the rise of the fan solidity, the high speed exhaust jet can flow to crash the pressure surface of the blade. Thus, the lift of the blade can be reduced in the 30% blade spanwise region from the blade tip.

(2) Blade tip pitch angle:θ = 8°

The preliminary flow field around the blade is shown in Fig. 14. As shown in the Fig. 14, the exhaust jet passes under the downstream blade when the blade number is 20, indicating a slight influence on the blade circulation. For the case with 6 blade number, it is hard to find the wake of the exhaust jet because the exhaust jet has a large reflection angle and the distance between the blades is farther enough. The comparison of the pressure distribution on the blade surface of the tip-jet and reference cases in different blade spanwise sections are displayed in Fig. 15. It is found that the low pressure area on the suction surface of the blade with tip-jet is extended little further than that of the reference blade in both 6 and 20 blades cases. As the pitch angle increases, the downwash speed and the momentum of the mainstream is enlarged except blade stall situation. It weakens the entrainment impact of the exhaust jet to the upstream mainstream. The impact of the exhaust jet on the pressure distribution of the blade pressure surface is not obvious.

The mean pressure coefficient at the different spanwise sections of the blade is shown in Fig. 16. It is shown that the major different region of the pressure distribution between

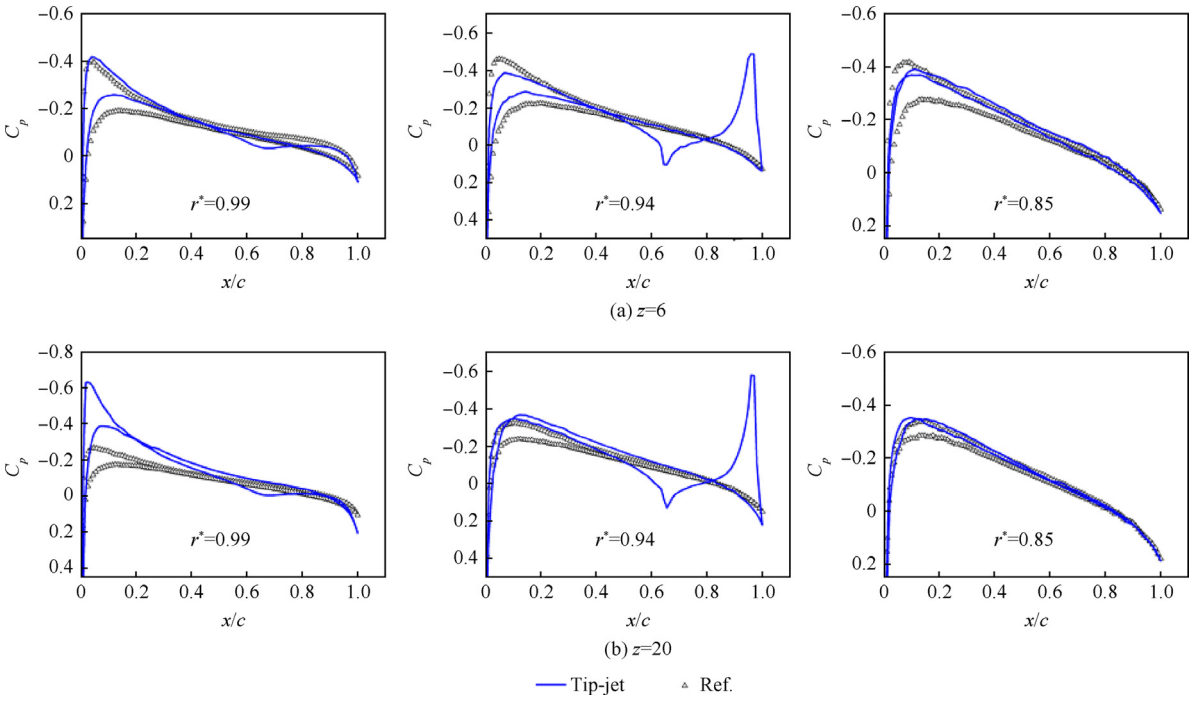

Fig. 13 Pressure distribution around blade section ($\theta = 2°$).

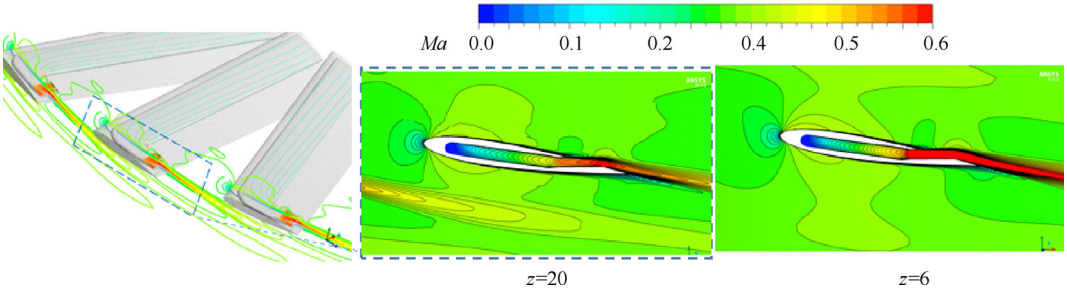

Fig. 14 Mach number contour around blade ($\theta = 8°$, ω_r = 3700 r/min).

the tip-jet and reference cases take up 15% spanwise region from the blade tip in both 6 and 20 blades cases. The pressure on the suction surface of the blade with tip-jet in this region is lower than that of the reference case, since the high speed jet reduces the pressure on the blade suction surface. The lowest pressure area at the pressure surface of the blade with tip-jet slightly moves to the tip direction but the lowest pressure value between the tip-jet and reference cases is close indicating a slight impact from the exhaust jet. The more details of the pressure distribution around the blade surface at the nozzle center in spanwise direction are shown in Fig. 17. The low pressure region at the rear part and suction surface of the blade is formed by the Coanda effect.

In brief, the lift of the tip-jet blade can be enlarged primarily in the nozzle spanwise region due to the pressure reduction on the suction surface of the blade when the blade number is 6 or 20 and the blade tip pitch angle is 8°. The same analysis method is employed in the configurations operating under 6300 r/min, and the similar flow features and aerodynamic changes are observed, showing less sensitivity to the rotational frequency. Hence, for brevity, only the discussions for the cases with ω_r = 3700 r/min have been presented. Nevertheless, the aerodynamic performance of the cases with ω_r = 6300 r/min is to be presented in the following section.

4.3. Aerodynamic performance

The impacts of the tip-jet and exhaust jet on the blade circulation eventually reflect on the fan's overall performance. Fig. 18 (a) depicts the thrust coefficient ratio ($C_T^* = (C_T - C_{Tr})/C_{Tr}$, C_{Tr} is the thrust coefficient of the reference fan) of the fans. The solid and hollow symbols represent the cases with 3700 r/min and 6300 r/min, respectively. As shown in Fig. 18 (a), the thrust of the fans with tip-jet is nearly 6% larger than that of the references cases in a wide range of the fan solidities when θ = 8°. The entrained flow on the suction surface of the blade contributes most to this augmentation. However, for θ = 2°, the thrust of the fans with tip-jet is gradually reduced with the rise of the fan solidity due to the impact of the exhaust jet from upstream. This reduction reaches 30% of the reference's thrust under the fan solidity of 0.7. However, under

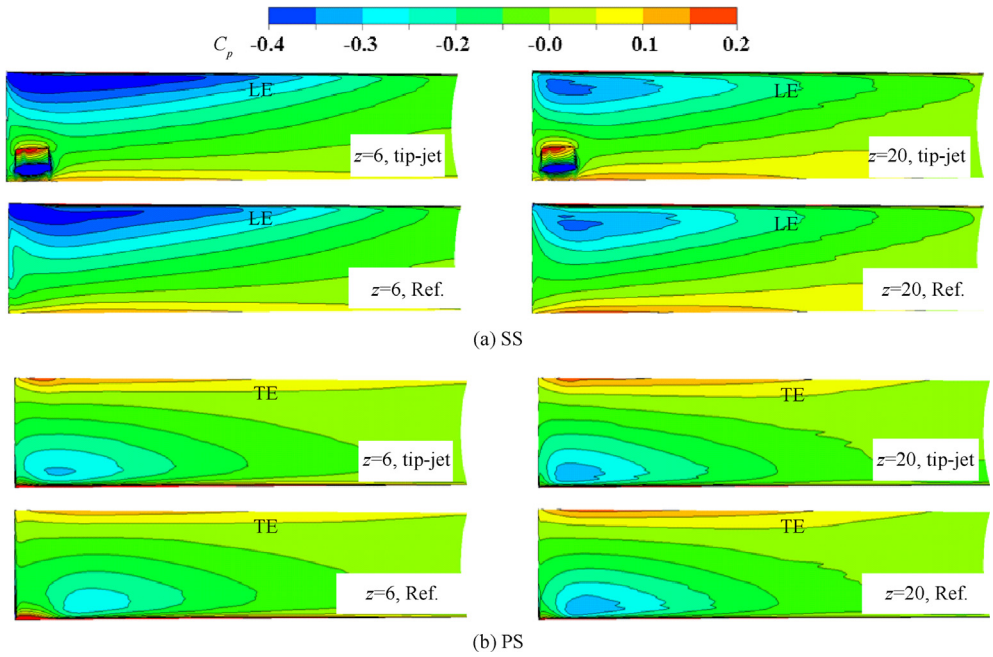

Fig. 15 Pressure distribution on blade surface ($\theta = 8°$).

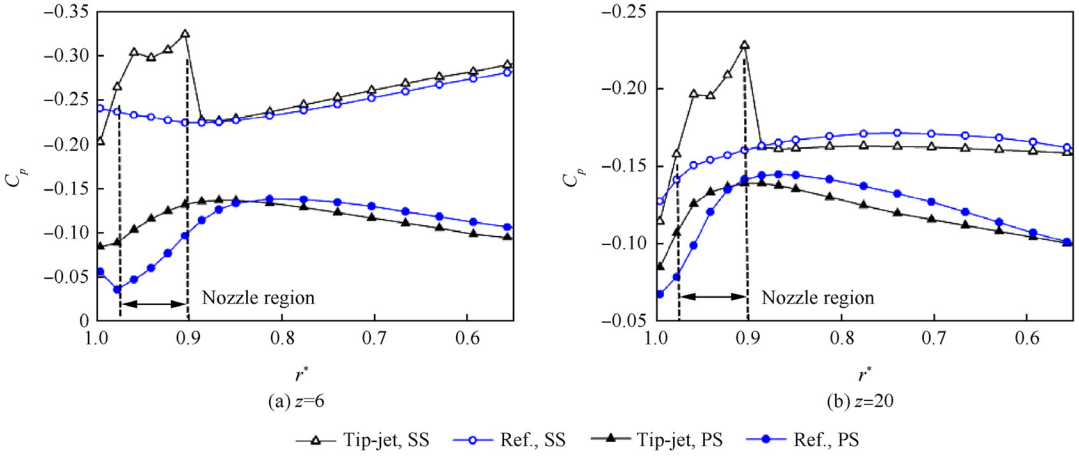

Fig. 16 Pressure distribution at blade spanwise direction ($\theta = 8°$).

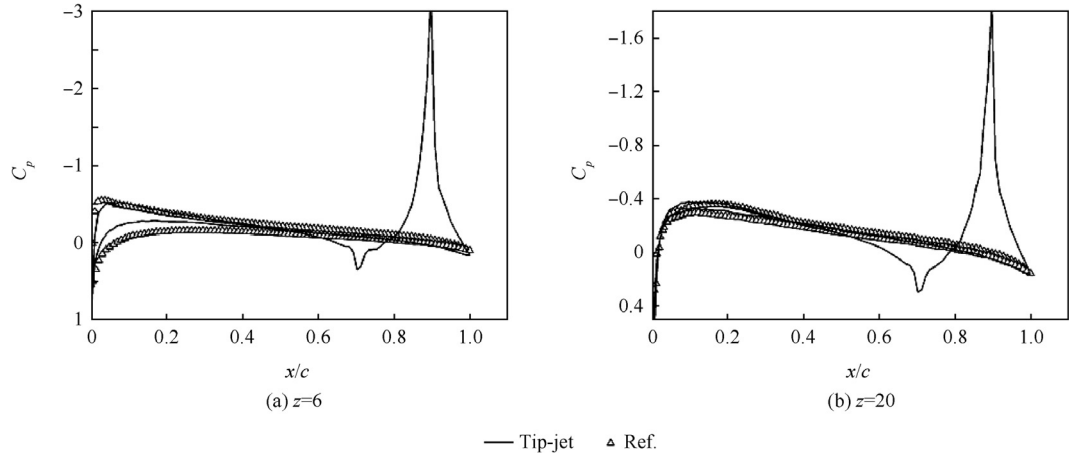

Fig. 17 Pressure distribution around blade section ($\theta = 8°$, r* = 0.94).

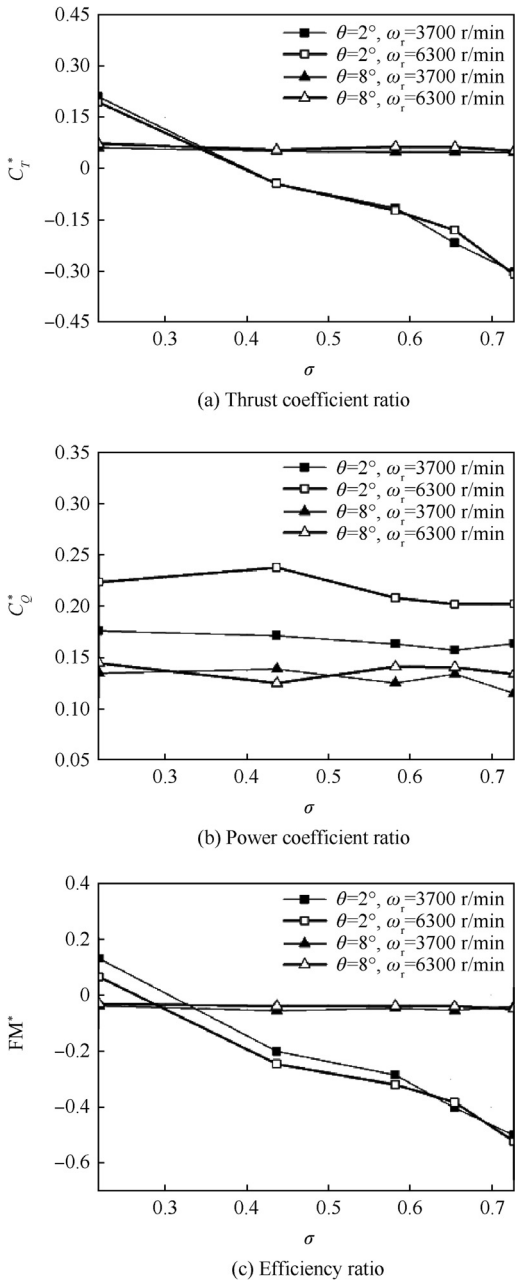

(a) Thrust coefficient ratio

(b) Power coefficient ratio

(c) Efficiency ratio

Fig. 18 Comparison of aerodynamic performance.

the condition of a lower fan solidity, the thrust augmentation is enlarged with the decrease of the pitch angle.

Fig. 18(b) depicts the power coefficients ratio ($C_Q^* = (C_Q - C_{Q\mathrm{r}})/C_{Q\mathrm{r}}$, $C_{Q\mathrm{r}}$ is the power coefficient of the reference fan) of the fans. The power of the tip-jet cases is nearly 13.5% larger than the reference cases at $\theta = 8°$. When $\theta = 2°$, the rising of the power of the tip-jet cases are nearly 17% and 21% under $\omega_\mathrm{r} = 3700$ r/min and $\omega_\mathrm{r} = 6300$ r/min, respectively. Such ratio declines slowly with the rise of the fan solidity. Fig. 18(c) depicts the efficiency ratio ($\mathrm{FM}^* = (\mathrm{FM} - \mathrm{FM_r})/\mathrm{FM_r}$, FM is the tip-jet fan's figure of merit and $\mathrm{FM_r}$ is the reference fan's figure of merit) of the fans. The trend of the fan efficiency ratio is similar to the thrust coefficient ratio. The efficiency of tip-jet cases is nearly 4% smaller than that of reference cases at $\theta = 8°$, under a wide range of the fan solidities. When $\theta = 2°$, the efficiency ratio is nearly reduced from 0.1 to −0.5 with the rise of the fan solidity from 0.2 to 0.7. It is suggested that the fan' s performance can be improved using the tip-jet technology when the fan solidity and pitch angle are both small. But this case cannot produce a high disk loading. The fan' s performance is worse with the rise of fan solidity at $\theta = 2°$. In practice, the pitch angle of fan could be larger than 8° to produce a high thrust. In that case, the flow direction of the exhaust jet can be deflected resulting in a slight impact on the downstream blade. Thus, the fan' thrust can be augmented in a large range of the fan solidity for the entrained mainstream on the suction surface of the blade. Besides, the nozzle can be mounted with an angle to avoid the exhaust jet crashing to the downstream blade. The most meaningful conclusion is that it is possible to apply the tip-jet in a high solidity and high pitch angle fan and without an adverse impact on the fan's aerodynamic performance.

5. Conclusions

(1) When the nozzle is on the suction surface of the blade, the flow direction of the exhaust jet can be deflected to attach the blade surface. The major exhaust jet decay region can extend at least 2 times the blade chord downstream from the blade trailing edge, in which the decline of the exhaust jet velocity is quick along the jet central trajectory. After that region, the decline of the exhaust jet velocity is slow. The margin of the jet influence region can extend at least 3.5 times downstream from the blade trailing edge. When the exhaust jet expands to the distance of 2 times the blade chord downstream from the blade trailing edge, the spreading width of the exhaust jet along the central trajectory is 0.1 times that of the blade chord.

(2) The exhaust jet could have a slight influence on the downstream blade in a high pitch angle fan, since the flow direction of exhaust jet can be deflected by the Coanda effect and the nozzle can be mounted with an angle. When the blade pitch angle is 8° and the fan solidity is less than 0.7, the fan's performance is impacted by the tip-jet on the blade rather than the exhaust jet from upstream. When the blade pitch angle is 8° in this paper, the fan's thrust can be augmented approximate 6% in comparison with to the fan without tip-jet, due to the pressure reduction on the suction surface of the blade. It is possible to apply the tip-jet in a high solidity and high pitch angle fan and without an adverse impact on the fan's aerodynamic performance.

(3) The exhaust jet has a slight influence on the downstream blade in a low solidity fan when the distance between the blades is larger than the major expanding margin of the exhaust jet. When the fan's solidity and pitch angle are both small, the fan' performance can be risen for the entrainment above the blade suction surface. When the blade tip pitch angle is small, and the fan solidity is high, the blade pressure surface can be crashed by the exhaust jet from upstream resulting in an adverse impact on the blade circulation. When the blade tip pitch angle is 2° in

this paper, the thrust ratio between the fans with and without tip-jet is reduced from 0.2 to −0.3, with the increase of the fan solidity from 0.2 to 0.7.

References

1. Roos FW. Mr. Mac's helicopters. Reston: AIAA; 2003. Report No.: AIAA-2003-0290.
2. Kestner BK, Tai JCM, Mavris DN. A computationally efficient methodology for generating training data for a transient neural network of a tip-jet reaction drive system. *J Eng Gas Turbines Power* 2011;133(12): 121601.
3. Armutcuoglu O, Kavsaoglu MS, Tekinalp O. Tilt duct vertical takeoff and landing uninhabited aerial vehicle concept design study. *J Aircraft* 2004;**41**(2):215–23.
4. Mitchell CA, Vogel BJ. The Canard Rotor Wing (CRW) aircraft—A new way to fly. Reston: AIAA; 2003. Report No.: AIAA-2003-2517.
5. Kong C, Park J, Kang M. A study on transient performance characteristics of the canard rotor wing type unmanned aerial vehicle propulsion system during flight mode transition. *J Eng Gas Turbines Power* 2006;**128**(3):573–8.
6. Phillips JD. An efficient tip jet drive. Reston: AIAA; 1991. Report No.: AIAA-1991-3124.
7. Schwartz AW, Reader KR, Rogers EO. An unmanned air vehicle concept with tip-jet drive. *J Am Helicopter Soc* 1994;**39**(3): 67–74.
8. Schwartz AW, Rogers E. Hover evaluation of an integrated pneumatic lift/reaction-drive rotor system. Reston: AIAA; 1992. Report No.: AIAA-1992-0630.
9. Holloway A, Richardson S. Development of a trailing vortex formed with spanwise tip jets. *J Aircraft* 2007;**44**(3):845–57.
10. Elmahmodi A, Davidovic N, Al-Madani RA. Propulsion system based on compressed air due to rotor blade rotation. *Int J Smart Grid Clean Energy* 2014;**3**(3):263–9.
11. Brentner KS, Morris PJ, Lopes LV. A method for predicting the noise of a tip-jet driven rotor. *J Am Helicopter Soc* 2014;**59** (3):1–10.
12. Zhao Q, Ma Y, Zhao G. Parametric analyses on dynamic stall control of rotor airfoil via synthetic jet. *Chin J Aeronaut* 2017;**30** (6):1818–34.
13. Barzegaran M, Kosari A. A model of flow separation controlled by dielectric barrier discharge. *Chin J Aeronaut* 2017;**30**(5):1660–9.
14. Zhang X, Huang Y, Wang X, Wang W, Tang K. Turbulent boundary layer separation control using plasma actuator at Reynolds number 2000000. *Chin J Aeronaut* 2016;**29**(5):1237–46.
15. Chen J, Li L, Huang G. Numerical investigations of ducted fan aerodynamic performance with tip-jet. *Aerosp Sci Technol* 2018;**78**:510–21.
16. Xu H, Qiao C, Yang H. Active circulation control on the blunt trailing edge wind turbine airfoil. *AIAA J* 2018;**56**(2):554–70.
17. Tian Y, Zhang Z, Cai J, Yang L, Kang L. Experimental study of an anti-icing method over an airfoil based on pulsed dielectric barrier discharge plasma. *Chin J Aeronaut* 2018;**31**(7):1449–60.
18. Wang X, Xiang C, Najjaran H, Xu B. Robust adaptive fault-tolerant control of a tandem coaxial ducted fan aircraft with actuator saturation. *Chin J Aeronaut* 2018;**31**(6):1298–310.
19. Sheng C, Zhao Q. Numerical investigations of fan-in-wing aerodynamic performance with active flow control. *J Aircraft* 2017;**54**(6):2317–29.
20. Bi N, Sydney A, Kimmel K, Haas D. Experimental investigation of fan aerodynamic performance for fan-in-wing applications. *AHS 71st annual forum;* 2015 May 5–7; Virginia, USA. Fairfax: AHS; 2015. p. 161–73.
21. Menter FR. Two equations eddy viscosity turbulence models for engineering applications. *AIAA J* 1994;**32**(8):1598–605.
22. Thouault N, Breitsamter C, Adams NA. Numerical investigation of inlet distortion on a wing-embedded lift fan. *J Propul Power* 2011;**27**(1):16–28.
23. Hadidoolabi M, Ansarian H. Supersonic flow over a pitching delta wing using surface pressure measurements and numerical simulations. *Chin J Aeronaut* 2018;**31**(1):65–78.